5-17-2021

# Removal of Hexavalent Chromium by Encapsulated Chitosan-Modified Magnetic Carbon Nanotubes: Fixed-Bed Column Study and Modelling

Mian Muhammad-Ahson Aslam

Walter Den

Hsion-Wen Kuo

# Removal of Hexavalent Chromium by Encapsulated Chitosan-Modified Magnetic Carbon Nanotubes: Fixed-Bed Column Study and Modelling

*Mian Muhammad Ahson Aslam*[†], *Walter Den*[‡,*], *Hsion-Wen Kuo*[†,*]

[†] Department of Environmental Science and Engineering, Tunghai University, No. 1727, Section 4, Taiwan Boulevard, Xitun District, Taichung City, 407, Taiwan, R.O.C.

[‡] Department of Science and Mathematics, Texas A&M University-San Antonio, One University Way, San Antonio, Texas, 78224, U.S.A.

[*] Co-corresponding authors:

walter.den@tamusa.edu; 1(210)784-2815

hwkuo@thu.edu.tw; 886(4)2359-0121 ext. 3363

**Abstract**

A new type of composite adsorbent, encapsulated chitosan-modified magnetic carbon nanotubes (CS/MWCNTs/Fe) beads were used to remove Cr(VI) from aqueous solutions in a fixed-bed column. Among the various combination of operating parameters, we obtain a maximum volume of treated effluent (210 mL) under the following conditions: flow rate, 1 mL $min^{-1}$; bed height, 8 cm; feed Cr(VI) concentration, 30 mg $L^{-1}$; and solution pH, 4.0±0.2. The corresponding adsorption capacity was 1.54 mg $g^{-1}$ and the overall Cr(VI) removal efficiency was 54%. In characterizing the dynamics of the adsorption process and breakthrough profiles, we found that the Thomas model and the Yoon-Nelson model both accurately described the breakthrough curves under all experimental conditions, while the Adams-Bohart model was applicable only for an early phase of dynamic behavior $\left(\frac{C_t}{C_0} \leq 0.5\right)$ of the CS/MWCNTs/Fe beads column. Columns with shorter bed heights favored the global mass transfer rate, especially during the early breakthrough periods. Moreover, the bed depth service time (BDST) model was validated experimentally, enabling the prediction of service time of the adsorption bed at different outlet concentrations using hypothetical flow rates and inlet concentrations. Scaled-up study was performed to observe the column performance at higher throughputs. The high selectivity of Cr(VI) adsorption in the simulated wastewater in the presence of other heavy metals ($Cu^{2+}$ and $Cd^{2+}$) and background anion ($PO_4^{3-}$) suggests the applicability of CS/MWCNTs/Fe beads for Cr(VI) removal from industrial effluents.

Keyword: Chitosan, chromium removal, carbon nanotubes, alginate, water treatment, fixed bed adsorption

## 1. Introduction

Chromium (Cr) is widely used in various industrial segments such as metallurgy, tanning and electroplating processes. It is one of the highly toxic heavy metals in water systems even at parts-per-billion levels [1], mostly due to the illicit or incidental discharge from industrial sources. The strong solubility and diffusivity of hexavalent chromium (Cr(VI)) that exist in the form of chromate ($CrO_4^{2-}$), hydrogen chromate ($HCrO_4^-$) and dichromate ($Cr_2O_7^{2-}$) in aqueous phase facilitates the compound to penetrate tissue membrane [2]. Trivalent chromium Cr(III), which at minute concentrations is regarded non-toxic, is another environmentally important Cr species that becomes harmful at high concentrations [3]. The metal ions can be removed from different environmental matrices by using techniques such as ion exchange, chemical precipitation [4], adsorption [5], coagulation [6], bio-reduction [7] and reverse osmosis [8]. Among these approaches, adsorption has been the method of choice for large-scale applications due to its process readiness, cost effectiveness, and design versatility [9].

A variety of adsorbents have demonstrated the ability to uptake Cr(VI) and other metal ions in the contaminated water. The sorbent materials include pyrolyzed biomass residues, biosorbents, activated carbons, graphene oxide, synthetic polymer and other nanoparticles [10]. A wide variability in the adsorption rate of several adsorbents has been reported in recent literature. Factors affecting the reported performance include solution pH, Cr(VI) concentration, temperature, ionic strength and potential interference of co-existence pollutants. For example, adsorption capacities of magnetite particles prepared from titanium residue, chitosan nanofiber and polypyrrole nano-membrane were recorded to be 14.5 mg $g^{-1}$ [11], 131.6 mg $g^{-1}$ [12], and 250 mg $g^{-1}$ [13], respectively. While the co-presence of $Cl^-$, $PO_4^{3-}$, $SO_4^{2-}$, As(III) and As(V) ions did not

impact the high Cr(VI) selectivity of magnetite particles prepared from titanium residues, the presence of fluoride led to a perceptible reduction in the selectivity [11].

While most commercial sorbents are used in their natural form, recent material advances trend towards modifying functional components by crosslinking and grafting to improve both adsorption performance and regeneration. Such engineered composite materials aim to either increase adsorption sites or to be selective to a specific contaminant in water. For instance, researchers have identified several types of adsorbents for Cr uptake with excellent selectivity, high uptake capacity and fast adsorption kinetics at low Cr(VI) concentrations. These materials include electrospun-polyacrylonitrile/carbon nanotubes/amine-functionalized titanium dioxide nanoparticles [14], amino functionalized polymer grafted with mesoporous silica [15], magnetic mesoporous $TiO_2$ core-shell microspheres immobilized with graphene oxide [16], and chitosan-g-maleic anhydride-ethylene dimethacrylate adsorbent [9]. Our research group recently prepared and characterized an encapsulated chitosan-modified, magnetic multi-walled carbon nanotubes (CS/MWCNTs/Fe) beads for aqueous phase Cr(VI) [17]. The Cr(VI) adsorption capacity of 119 mg $g^{-1}$ was achieved using batch adsorption experiments.

Although the adsorbents mentioned above have demonstrated excellent adsorption capacities in sequestering Cr species from aqueous solutions, most of the experiments were performed in batch modes to characterize the equilibrium isotherms and adsorption kinetics. Adsorption parameters acquired from batch studies, however, may not be sufficient to determine the performance in treatment systems operated in continuous-flow column and completely-mixed modes [18]. Several researchers have reported that the fixed-bed adsorption systems are the most effective method of adsorption-desorption cycles, because such systems can elucidate the effects of the concentration gradient (i.e., adsorption driving force). In addition, fixed-bed adsorption

systems also have many process design advantages, including high-volume operations and can be systematically scaled between bench and industrial units [19].

The present study aimed to assess the Cr(VI) uptake performance of CS/MWCNTs/Fe beads in continuous fixed-bed columns using different parameters such as flow rate, bed depth, feed Cr(VI) concentration, and solution pH values. Several empirical models that have been used to characterize the adsorption of heavy metal ions, namely the Thomas model [20, 21], Adams-Bohart (A-B) model [22, 23], and Yoon-Nelson (Y-N) model [24, 25], are applied to fit the experimental data. These models describe the breakthrough curves and obtain design process parameters such as adsorption kinetics and maximum uptake capacity. Furthermore, the Bed Depth Surface Time (BDST) model is applied to analyze the service time of adsorbent bed at different outlet concentrations and to obtain data for scale-up purposes. We evaluated the Cr(VI) adsorptivity when challenged with a mixture of heavy metals (copper, cadmium) and an anions (phosphate) in the simulated wastewater representative of metal-plating process discharges. The adsorption capacity, adsorbent breakthrough, saturation rate, and processed bed volume are used as performance indicators of the CS/MWCNTs/Fe beads.

## 2. Material and Methods

### 2.1 Preparation and characterization of composite beads

The composite beads used for Cr(VI) adsorption have previously been prepared and characterized in detail in our recent work [17]. Briefly, as-received MWCNTs were impregnated in a 1:3 v/v mixture of reagent-grade acids containing $H_2SO_4$ and $HNO_3$ (5 M) at 100˚C to remove any organic impurities and to functionalize the surface with hydroxyl and carboxyl groups. The product was then filtered and washed with deionized water (DIW) until pH neutrality was reached

and then oven-dried at 80˚C for 12 h. To prepare the iron-laden MWCNTs, the conditioned MWCNTs were re-suspended in DIW (1 g $L^{-1}$) under sonication for 1 h. To this, a solution mixture (2:1 molar ratio) containing $FeCl_3 \cdot 6H_2O$ (4 mL) and $FeSO_4 \cdot 7H_2O$ (1 mL) was added gradually, followed by dropping ammonium hydroxide to adjust the pH value to about 10. The magnetically precipitated iron-laden MWCNT particles were rinsed with ethanol, oven-dried for the ensuing steps.

CS/MWCNTs/Fe particles were prepared by dissolving purified chitosan (CS) (medium molecular weight, Sigma-Aldrich, Germany) in DIW containing 2% (v/v) acetic acid (10 g $L^{-1}$). The solution was gradually mixed with MWCNTs/Fe suspension (10 g $L^{-1}$) followed by adding galatraldehyde as the crosslinking agent. The prepared CS/MWCNTs/Fe nanoparticles were encapsulated by alginate beads by adding 10 g CS/MWCNTs/Fe particles to sodium alginate solution (10 g $L^{-1}$). The mixture was injected into 200 mL of calcium chloride solution (50 mM) at a rate of 0.01 L $h^{-1}$ while gently stirring for 12 hours to allow crosslinking of $Ca^{2+}$ with sodium alginate to form CS/MWCNTs/Fe beads. Finally, the collected beads were washed, air dried and stored for further use in adsorption experiment.

Different stock solutions of Cr(VI), Cu(II), Cd(II) and phosphate anions (1,000 mg $L^{-1}$ each) were prepared by dissolving 2.8287 g of $K_2Cr_2O_7$, 3.9293 g of $CuSO_4.5H_2O$, 2.7442 g of $Cd(NO_3)_2$ and 2.2350 g of $K_3PO_4$ in 1.0 L of DIW, respectively. Further the required samples were prepared by diluting the stock solutions to a desired concentration. The pH of these sample solutions was adjusted to a specified value using 1 M $H_2SO_4$ and NaOH solutions. All the chemicals used in this study were of reagent grade.

**2.2 Fixed-bed adsorption studies**

Fixed-bed adsorption tests were performed using a glass column of 14 cm in length and 2 cm in internal diameter. The column studies were operated using the following range of parameters: Flow rate, 1, 2, 3, and 4 mL $min^{-1}$; bed depth, 4, 6, and 8 cm; feed Cr(VI) concentration, 30, 50, and 100 mg $L^{-1}$; pH, 2, 4, 6 and 8. After packing with the CS/MWCNTs/Fe beads to a prescribed height, the Cr(VI) solution of predetermined concentrations and pH were fed to the column using a peristaltic pump (EYELA MP-2000, Japan) with a specified flow rates in the downward direction. The effluent samples collected after a specified time interval at the outlet of the column were tested for residual Cr(VI) ions through a spectrophotometry (T60UV-Visble Spectrophotometer, U.K.) using diphenylcarbazide as colorimetric reagent at the wavelength of 540 nm [26].

Among several important factors that affect the feasibility of a fixed-bed adsorption system, the potential interference of coexisting pollutants that usually contain other anionic and cationic pollutants in industrial wastewater effluent is also very important. For this reason, the simulated wastewater was used as the column feed and column adsorption process experiments were conducted for the simultaneous uptake of Cr(VI), Cu(II), and Cd(II) at an initial feed concentration of 1 mg $L^{-1}$ each. Other standard experimental conditions were 30 mg $L^{-1}$ of phosphate as background anions, a flow rate of 1 mL $min^{-1}$, a bed depth of 8 cm and a solution pH of 4±0.2. The concentration of total chromium, Cu(II) and Cd(II) was measured by an inductively-coupled plasma/mass spectrometer (Model 7800 ICP-MS, Agilent, U.S.A.).

**2.3 Determination of adsorption breakthrough curves**

The performance evaluation of the fixed-bed column was studied based on the breakthrough behavior obtained by plotting $C_t/C_0$ (effluent-to-influent ratio) versus time t. The bed breakthrough and saturation were defined as the times for which the value of $C_t/C_0$ reaches 5%

and 95%, respectively. The total Cr(VI) adsorbed in the adsorbent bed, $q_{total}$ (mg), is determined through the following equation:

$$q_{total} = \frac{Q}{1000}\int_{t=0}^{t=t_{total}} C_{ad}\, dt \quad (1)$$

where Q (mL $min^{-1}$) is the volumetric flow rate, $t_{total}$ (h) is the total time of flow, and $C_{ad}$ (mg $L^{-1}$) is the difference in total Cr(VI) ions at initial time and the time t caused by the adsorption in the column (i.e., $C_{ad} = C_0 - C_t$). Here, the adsorption capacity of adsorbent bed, $q_e$ (mg $g^{-1}$), and the equilibrium concentration of Cr(VI) ions, $C_e$ (mg $L^{-1}$), are calculated as follows:

$$q_e = \frac{q_{total}}{W} \quad (2)$$

$$C_e = \frac{1000\,(m_{total} - q_{total})}{Qt_{total}} \quad (3)$$

where W (g) is the amount adsorbent packed in the column, and $m_{total}$ (mg) is the amount of total Cr(VI) ions passing through the column (i.e., $m_{total} = \frac{C_0 Q t_{total}}{1000}$). The fractional removal of Cr(VI) ions, R (%), can be expressed as the ratio of $q_{total}$ and $m_{total}$.

Other parameters associated with fixed-bed column characterizations are the linear flow velocity, v (cm $min^{-1}$), the empty bed contact time, EBCT (h), and the length of mass transfer zone, MTZ (cm). They are determined as follows:

$$v = \frac{Q}{A} \quad (4)$$

$$EBCT = \frac{\text{Volume of bed}}{Q} \quad (5)$$

$$MTZ = \frac{Z\,(t_e - t_b)}{t_e} \quad (6)$$

where A ($cm^2$) is the is the cross-sectional area of the column, Z (cm) is the bed height, and $t_b$ and $t_e$ (h) are the column breakthrough and saturation times, respectively.

### 2.4 Empirical adsorption breakthrough models

The adsorption dynamics of a fixed-bed column can be described by using suitable models fitted on the experimental data necessary for the scale-up proposes and performance comparison. Multiple mass transport factors, such as the adsorption kinetics, axial dispersion, film mass transfer resistance, and intraparticle diffusion limitations, are involved in the fixed-bed adsorption process, complicating the adsorption process. It necessitates the use of a set of nonlinear partial differential equations to simulate phenomenologically the process steps and to predict the breakthrough behavior of adsorption columns. Nevertheless, fixed-bed adsorption models usually exhibit some discrepancies between experimental and predicted data, and empirical models are valuable in simplifying the process conceptualization to adequately characterize column breakthroughs. These empirical models include the Thomas model, Y-N model and A-B model. Furthermore, the Mass Transfer Factor (MTF) models were applied to determine the mass transfer resistance from the adsorption of Cr(VI) onto CS/MWCNTs/Fe beads packed in the column. The BDST model was also fitted to estimate the kinetic parameters depicting the relationship between bed depth and service time. The model equations, key assumptions and characteristics are summarized in Table 1 (Detail narratives can be found in Supplementary Text S-1.) The models' parameters were obtained by linear and non-linear regression fit. A nonlinear curve fitting was obtained using the regression tool (Solver-add in) in MS-Excel based on the magnitude of the coefficient of the determination ($r^2$) by minimizing the value of sum of squared error (SSE). In this study, standard error (SE) and SSE were used as instruments to measure the degree of model fits with the experimental values. The expression for SE and SSE analysis are as follows:

$$SE = \sqrt{\frac{\sum(C_{cal} - C_{exp})^2}{N}} \quad (7)$$

$$SSE = \sum\left(C_{cal} - C_{exp}\right)^2 \quad (8)$$

where $C_{cal}$ and $C_{exp}$ are the calculated and experimental outlet concentrations respectively in terms of $C_t/C_0$ and N is the experimental observations.

***Mass Transfer Factor model***

The MTF models were employed to analyze the global, internal and external mass transfer resistance from the adsorption onto the surface of adsorbent [27, 28] at different bed heights of the column. The external mass transfer coefficient can be expressed:

$$ln\left(\frac{C_0}{C_t}\right) = [k_L a]_f \times t \quad (9)$$

where, $[k_L a]_f$ indicates the external or film or volumetric film mass transfer coefficient ($h^{-1}$), $k_L$ (m $h^{-1}$) is the mass transfer coefficient, a ($m^{-1}$) is the surface interfacial liquid-solid and t (h) is the time of water fed to the column.

The relationship between the external and the global mass transfer coefficients can be expressed as follows [27, 28]:

$$[k_L a]_f = [k_L a]_g \times e^{-\beta \times \ln(q)} \quad (10)$$

By substituting Eq. 10 into Eq. 9, the following relation can be obtained:

$$ln\left(\frac{C_0}{C_t}\right) = [k_L a]_g \times e^{-\beta \times \ln(q)} \times t \quad (11)$$

where $[k_L a]_g$ is global mass transfer coefficient ($h^{-1}$), β (g $h^{-1}$ $mg^{-1}$) is the absorbate-adsorbent affinity and q (mg $g^{-1}$) is the is quantity of the Cr(VI) to adsorb by the CS/MWCNTs/Fe beads.

The mathematical deduction and linearization of Eq. 11 leads to:

$$ln(q) = B + \frac{1}{\beta} \times \ln(t) \quad (12)$$

where B (mg $g^{-1}$) indicates the potential mass transfer index relating to the driving force for mass transfer

$$B = \frac{\ln([k_L a]_g) - \ln\left\{\ln\left(\frac{C_0}{C_t}\right)\right\}}{\beta} \quad (13)$$

The porous diffusion can be represented as the difference between global and external mass transfer factors:

$$[k_L a]_d = [k_L a]_g - [k_L a]_f \quad (14)$$

here, $[k_L a]_d$ is the porous diffusion factor ($h^{-1}$).

## 3. Results and Discussion

### 3.1 Effect of operating parameters

Fig. 1 shows the adsorption capacity and saturation time (i.e., time needed to achieve a 95% breakthrough) when one of the operating parameters are varied. The baseline conditions were: flow rate, 1 ml $min^{-1}$; bed height, 8 cm; feed Cr(VI) concentration, 30 mg $L^{-1}$; and solution pH, 4.0±0.2.

As shown in Fig. 1a, when the flow rate was increased from 1 to 2 mL $min^{-1}$, the Cr(VI) adsorption capacity of CS/MWCNTs/Fe beads increased from 1.52 mg $g^{-1}$ to 1.79 mg $g^{-1}$ while the saturation time decreased from 11.5 h to 6.0 h. The increasing flow rates in this range led to both an increased mass loading and a reduced residence time for the Cr(VI) solution in the column,

thereby causing the increased adsorption capacity and reduced saturation time. Further increases in flow rates, however, resulted in only a marginal change in both adsorption capacity and saturation time (Table S-1). As the Reynolds numbers (0.8 to 3.0) corresponding to the flow rate changes stayed within the laminar regime, the effect of fluid turbulence on the external mass transfer resistance on the absorbent surface was minimal. However, the Peclet numbers have been reported to have a marked impact on mass transfer coefficients in packed beds when its value transitioned from <100 (at 1 ml $min^{-1}$ in this study) to >200 (at a flow rate >3 ml $min^{-1}$) [29]. Therefore, we reasoned that, reduced residence time was the primary factor for the observed shorter saturation time, however, the effects of increased mass transfer resistance at a greater flow velocity may have compromised the adsorption capacity as flow rate increased. Of note, our recent study on batch adsorption experiments exhibited much higher equilibrium adsorption capacity (119 mg $g^{-1}$) than the value observed in column tests, demonstrating that mass transfer process in continuous-flow column operations represents a limiting factor in the adsorption of Cr(VI) ions by the CS/MWCNTs/Fe beads in fixed-bed column system. Additionally, as the flow rate increases, the effluent volume at breakthrough time ($V_B$) decreases, while the effluent volume at time of saturation ($V_S$) increases. For example, at the flow rate of 2 mL $min^{-1}$, the maximum removal efficiency reached 55% with a $V_B$ of 180 mL, as compared to a removal rate of 53% and a $V_B$ of 210 mL at a flow rate of 1 mL $min^{-1}$. The increase in Cr(VI) removal efficiency with increasing flow rate from 1 to 2 mL $min^{-1}$ is attributed to the MTZ expansion from 5.6 to 6.0 cm (Details of calculation shown in Table S-1). These results corroborated with those described with the pattern of adsorption capacities at the various flow rates.

When the bed depth was increased from 4 cm to 8 cm, the adsorption capacity increased from 0.60 mg $g^{-1}$ to 1.52 mg $g^{-1}$, as shown in Fig. 1b. Also, the saturation time extended from 3.5

h to 11.5 h (Fig. 1b). The increase in the saturation time can also be attributed to a longer MTZ (3.4 to 5.6 cm) and EBCT (0.21 to 0.42 h) with the increment in bed depth. The reduced adsorption capacity with the smaller bed depth was owing to the formation of a slow and shortened MTZ that magnifies the adverse effect of axial dispersion, resulting in the reduced diffusion of Cr(VI) ions into the adsorbent beads. Cr(VI) removal efficiency increased from 27.0 to 53.6 % for increasing adsorbent bed height from 4 to 8 cm (Table S-1). Summarily, a longer bed depth is desired for improved adsorption capacity.

Fig. 1c shows that, when the feed concentrations were 30, 50 and 100 mg $L^{-1}$, the adsorption capacities were 1.52 mg $g^{-1}$, 1.22 mg $g^{-1}$, and 1.40 mg $g^{-1}$, and the corresponding saturation times were about 11.5 h, 6.0 h and 4.5 h. Furthermore, with increasing in inlet Cr(VI) concentration (30 to 100 mg $L^{-1}$), the breakthrough time and removal efficiency the bed decreased from 3.5 h to 0.5 h and from 53.6 % to 35.1 %, respectively (Table S-1). It is worth noting that a considerable increase in concentration provide a higher driving force and crowding of the diffusion path of Cr(VI) which leads to fast mass transfer of Cr(VI) ions into the CS/MWCNT/Fe beads and increases the competition between metal ions which ultimately results in to quick breakthrough and rapid saturation.

Solution pH is important to study because it greatly influence the ionic state of Cr species and active sites present in the adsorbent that governs the pattern of adsorption. Fig. 1d shows that, at the solution pH of 2, 4, 6, and 8, the saturation times were 7.5 h, 11.5 h, 6.0 h, and 3.0 h; and the corresponding adsorption capacities were 1.01 mg $g^{-1}$, 1.52 mg $g^{-1}$, 0.70 mg $g^{-1}$, and 0.26 mg $g^{-1}$, respectively. The longer saturation time and higher adsorption capacity observed for the solution at the pH of 4±0.2 revealed that the protonated groups ($–COOH_2^+$, $–OH_2^+$ and $–NH_3^+$) present in CS/MWCNTs/Fe beads are capable of capturing the Cr(VI) ions present in the solution

in the form of $HCrO_4^-$, resulting in the higher removal of metal ions in acid regime (i.e., pH 4). Therefore, pH 4 was taken as the optimum value for Cr(VI) adsorption in other column experiments. These trends matched well with those of the batch experiments reported in our prior study [17].

### 3.2 Adsorption breakthrough modeling

Fig.s 2a-d show the experimental breakthrough profiles for Cr(VI) adsorption using the various operating parameters delineated earlier. These experimental profiles were fitted with the Thomas model (curves in blue), Y-N model (red) and A-B model (green). The fitted model constants are summarized in Supplemental Materials (Table S-3). For all model fittings, nonlinear regression analysis provided higher accuracy as determined by SE (ranging from $7\times10^{-9}$ to $1\times10^{-3}$ for the Thomas model and the Y-N model; $7\times10^{-7}$ to $2\times10^{-4}$ for the A-B model) and by SSE ($9\times10^{-3}$ to $1\times10^{-2}$ for the Thomas model and the Y-N model; $4\times10^{-4}$ to $1\times10^{-2}$ for the A-B model). The $r^2$ value ranged from 0.981 to 0.999 for the Thomas model and Y-N model, and from 0.944 to 0.993 for the A-B model. Note that the A-B model only fits well for the early phase of breakthrough curve $\left(\frac{C_t}{C_0} \leq 0.5\right)$, and that the Thomas model and the Y-N model share identical mathematical form, hence the identical regression accuracies.

Despite taking the same mathematical form, the parameters in the Thomas model and the Y-N model offer different interpretations. For the Thomas model, as the flow rate increases (1 to 4 mL $min^{-1}$), the $k_{TH}$ value also increases (0.021 to 0.054 L $h^{-1}$ $mg^{-1}$) owing to the diminished mass transport resistance with the increased in flow rates [30]. Moreover, with the initial increase in the flow rate from 1 to 2 mL $min^{-1}$, the $q_{TH}$ value also increase from 1.64 to 2.07 mg $g^{-1}$, then it remains steady on further flow rate increase. Additionally, with increasing bed depth from 4 cm to 8 cm

leads to a decrease in $k_{TH}$ value from 0.054 L $h^{-1}$ $mg^{-1}$ to 0.021 L $h^{-1}$ $mg^{-1}$, whereas, $q_{TH}$ values increases from 0.78 mg $g^{-1}$ to 1.64 mg $g^{-1}$. When Cr(VI) feed concentration increases from 30 mg $L^{-1}$ to 100 mg $L^{-1}$, the $k_{TH}$ values remained in the range of 0.021 to 0.012 L $h^{-1}$ $mg^{-1}$, while the $q_{TH}$ values remained relatively constant between 1.64 and 1.73 mg $g^{-1}$. The behaviors of $k_{TH}$ and $q_{TH}$ with respect to flow rate, bed depth, and feed concentration remain in parallel with what we presented in Fig. 1a-c. This is not the case for the two key parameters in the Y-N model, where the $k_{YN}$ value generally increases (from 0.62 $h^{-1}$ to 1.61 $h^{-1}$) with increasing flow rates, decreases (from 1.62 to 0.62 $h^{-1}$) with greater bed heights, and increases (from 0.62 to 1.29 $h^{-1}$) with feed concentrations. The $\tau$ value has the opposite trends as it is inversely proportional to $k_{YN}$.

As such, the Thomas model parameters ($k_{TH}$ and $q_{TH}$) have physical implications reflecting the mass transfer rate and adsorption capacity. For example, a larger value in $k_{TH}$ at lower Cr(VI) feed concentration indicates that the adsorption of Cr(VI) ions onto the CS/MWCNTs/Fe beads in packed bed columns was kinetically favorable at lower concentration. This model fits best for the conditions with minimal external and internal diffusion resistance. The high correlation values and the consistency of $q_{TH}$ with those of experiment values indicates that Cr(VI) adsorption mechanism by CS/MWCNTs/Fe beads follow Langmuir isotherm and pseudo-second order adsorption kinetics [30, 31]. In comparison, the Y-N model takes advantage of the symmetric nature of the equation and uses the first 50% column breakthrough to project the entire breakthrough pattern. In this study, the $\tau$ values determined by the model equation are very close to that of experimental values. Therefore, the Y-N model can be reliably used for predicting the saturation time of the CS/MWCNTs/Fe beads column.

For the A-B model, the value of $N_{AB}$ increases from 662.3 mg $L^{-1}$ to 913.2 mg $L^{-1}$ with an increased flow rate from 1 to 3 mL $min^{-1}$, followed by a decrease to 845.1 mg $L^{-1}$ upon further

increasing flow rate to 4 mL $min^{-1}$. In addition, the $k_{AB}$ value increases from 0.014 L $mg^{-1}$ $h^{-1}$ to 0.036 L $mg^{-1}$ $h^{-1}$ with the increased flow rate from 1 mL $min^{-1}$ to 4 mL $min^{-1}$, suggesting that the adsorption kinetics in the early part of the adsorption ($C_t/C_0$ = 0.5) is controlled by external mass transfer [32, 33, 34]. When bed height is expanded from 4 cm to 8 cm, the $N_{AB}$ value increases from 353.1 mg $L^{-1}$ to 662.3 mg $L^{-1}$, while the $k_{AB}$ value declines from 0.035 L $mg^{-1}$ $h^{-1}$ to 0.014 L $mg^{-1}$ $h^{-1}$. The increase in feed Cr(VI) concentration from 30 mg $L^{-1}$ to 100 mg $L^{-1}$ also leads to an increase in $N_{AB}$ value (from 662.3 mg $L^{-1}$ to 750.0 mg $L^{-1}$) but the $k_{AB}$ value decreases from 0.014 L $mg^{-1}$ $h^{-1}$ to 0.009 L $mg^{-1}$ $h^{-1}$. These results further support our earlier hypothesis that the film mass transfer control the adsorption kinetics of the system at the early phase of adsorption at a larger flow rate.

**3.3 Mass transfer analysis**

Using the MTF models [27, 28], the linearized plots of ln(q) versus ln(t) resulted in good correlation ($r^2$ > 0.96) that enables the determination of the value 1/β (slope) and of B (i.e., intercept). The values of B decreased from -1.58 to -1.86 mg $g^{-1}$ and 1/β from 1.12 to 1.05 g h $mg^{-1}$ with increment in bed heights from 4 to 8 cm, indicating that a shorter bed depth is advantageous for better mass transfer than longer depths.

To elucidate the controlling mass transfer factor, we plotted the global mass transfer coefficient and its two components (i.e., external and porous diffusion). Fig. 3a shows the rate of global mass transfer for the adsorption of Cr(VI) onto CS/MWCNTs/Fe beads. It is evident that, during early breakthrough periods ($C_t/C_0$ < 0.2), there were marked differences in the global mass transfer rate, favoring columns with shorter bed depths, i.e., $[K_L a]_g$ values in the order of 4 cm > 6 cm > 8 cm. Furthermore, the analysis of film transfer rate coefficient **(**Fig. 3b) and diffusion mass transfer coefficient (Fig. 3c) illustrate an opposite trend. All $[k_L a]_f$ profiles exhibited an

asymptotic pattern approaching zero when significant breakthroughs occurred, clearly impelled by the greater concentration gradient between the bulk solution and the solid surface in the early phase of breakthroughs. Moreover, we noted that significant film transfer occurred only in the limited breakthrough window ($C_t/C_0 < 0.05$) for the bed height of 8 cm, whereas a similar rate could still be observed at $C_t/C_0 \sim 0.4$ for the 4 cm packed column. Conversely, Fig. 3c reveals that the rate of pore diffusion ($[k_L a]_d$) that occurs once an ion penetrates the film and reaches the solid surface was greater for longer bed depths. While the reversal of the trend was largely a result of the differences in film transfer rate, another conceivable explanation for this result is that the interstitial hydrodynamics changed as the packed bed was extended. These analyses point to the fact that packing depth represents a design variable that influences the mass transfer rates and the Cr(VI) adsorption on CS/MWCNTs/Fe beads.

### 3.4 BDST Model and Column Scaleup

Fig. 4 reveals the of service time as a function of adsorbent bed height, using four saturation ratios ($C_t/C_0$ = 0.05, 0.25, 0.50, and 0.95). Fitting with the experimental data indicates a highly linear relationship ($r^2 > 0.98$). This result enables us to use the BDST model equation to estimate the model parameters ($N_0$ and $k_B$) via determining the slope ($a = \frac{N_0}{C_0 v}$) and intercept ($b = \frac{1}{k_B C_0} \mathrm{Ln}\left(\frac{C_0}{C_t} - 1\right)$) of the fitted linear curves. With the increase of $C_t/C_0$ from 0.05 to 0.95, the value of $N_0$ increased from 5.97 mg $L^{-1}$ to 19.10 mg $L^{-1}$ while the $k_B$ values decreased (calculated results can be found in Supplemental Table S-5). The parameter $N_0$ is the adsorption equilibrium capacity and $k_B$ is the adsorption rate, both dependent of the mass loading reflected by the presence of $C_0$ and v. A significant increase in $N_0$ value versus $C_t/C_0$ reflects the high adsorption capacity of the bed with increased mass loadings. Conversely, a decreasing $k_B$ value is indicative of slower

adsorption rate of Cr(VI) ions as the process approaches complete breakthrough. It is worth noting that, despite its simplicity for the prediction of breakthrough time, the BDST model may not be applicable for depicting the adsorption behavior over the entire breakthrough range because its symmetric nature of a logic function (i.e., S-shaped curve) does not match well with most breakthrough profiles. Consequently, the parameter values $N_0$ and $k_B$ at the extended breakthrough range should only be taken with limited contexts, such as observing its trend as opposed of using it as a design basis.

The high correlation between the experimental ($t_b$) and predicted breakthrough time ($t_c$) validates the applicability of BDST for this study. Therefore, we further applied the model to predict column performance at other hypothetical operating conditions (flow rates and feed concentrations) for Cr(VI) adsorption on to CS/MWCNTs/Fe beads in packed bed column. This prediction step can be achieved by establishing new values of slope (a') and intercept (b') proportional to the ratio of hypothetical and validated conditions in both $C_0$ and v:

$$a' = a\frac{v}{v'} = a\frac{C_0}{C_0'} \quad (15)$$

$$b' = b\frac{C_0}{C_0'}\frac{\ln(C_0'-1)}{\ln(C_0-1)} \quad (16)$$

The prediction utilizes $N_0$ and $k_B$ values determined from the same flow rate and feed Cr(VI) concentration to modify the BDST model. By using a hypothetical concentration ($C_0$' = 5 mg $L^{-1}$) and bed height (30 cm) at a low flow rate (1 mL $min^{-1}$), the predicted service time for $C_t/C_0$ = 0.05, 0.25, and 0.50 were about 118, 210, and 282 h, respectively. The service time decreased to 3.3, 5.9, and 7.85 h for the corresponding $C_t/C_0$ values upon increasing feed Cr(VI) concentration to 200 mg $L^{-1}$. Similarly, with a hypothetically high flow rate (10 mL $min^{-1}$) while maintaining identical feed concentration (5 mg $L^{-1}$) and bed height (30 cm), the predicted service time became

16.4, 29.1, and 38.5 h for the corresponding $C_t/C_0$ ratios. The predicted breakthrough time for new bed depth (Z'), feed concentration ($C_0$') and flow rate (Q') are listed in Table S-6.

The scale-up study was further extended by using the number-of-bed-volume (NBV) method, whose value can be calculated for particular experimental conditions such as flow rate, bed height and inlet Cr(VI) concentration. NBV can be expressed as [34]:

$$\text{NBV} = \frac{Volume\ of\ water\ treated\ till\ breakthrough\ point}{volume\ of\ the\ adsorbent\ bed} \quad (17)$$

At any bed height and cross-sectional area of the scaled-up column, the volume of treated effluent can be estimated by NBV times with the packed bed volume. The new packed bed volume can be obtained by changing the bed height and cross-sectional area of the column while maintaining one as a constant at a time. The breakthrough time can be estimated by using the obtained volume of effluent processed divided by the flow rate. For this study, the estimated amount of CS/MWCNTs/Fe beads required for packing the column to achieve the desired breakthrough time can be obtained by multiplying the bulk density (0.4718 g $cm^{-3}$, as measured by the cylinder method) of adsorbent with the volume of scaled-up bed. The calculations were executed at a feed Cr(VI) concentration (30 mg $L^{-1}$) and two flow rates (50 mL $min^{-1}$ and 100 mL $min^{-1}$). Fig. 5a shows the scaled-up column performance at varying bed depths (10 cm to 60 cm) while keeping the column diameter (10 cm) constant. The scaling criteria was selected on the basis of linear flow velocity (≤0.32 cm $min^{-1}$) as observed for the baseline conditions used in the lab-scale study. For example, 4.4 kg of adsorbent would be needed to obtain a breakthrough time of 26 h for a flow rate of 50 mL $min^{-1}$, and 13 h for 100 mL $min^{-1}$. Similarly, 8.8 kg would be required to extend the breakthrough time to 53 h for a flow rate of 50 mL $min^{-1}$, and 26 h for 100 mL $min^{-1}$. Conversely, one can estimate the breakthrough time by varying the column diameter (10 cm to

20 cm) while maintaining a constant bed height (30 cm). For example, Fig. 5b indicates that 6.4 kg of adsorbent would be needed to pack a column with a diameter of 14 cm to obtain a breakthrough time of 52 h at a flow rate of 50 mL $min^{-1}$, and 26 h at 100 mL $min^{-1}$. When the column diameter is increased to 20 cm, 17.8 kg would be required to achieve a breakthrough time of 105 h at 50 mL $min^{-1}$ and 53 h at 100 mL $min^{-1}$.

### 3.5 Applicability of CS/MWCNTs/Fe beads fixed-bed column in treating a simulated effluent

The simultaneous uptake of three metal ions Cr(VI), Cu(II) and Cd(II), each at a feed concentration of 1 mg $L^{-1}$ by the fixed-bed columns packed with CS/MWCNTs/Fe beads was investigated in the presence of phosphate (30 mg $L^{-1}$) as a background anion. The pH of the simulated effluent was kept at 4.0±0.2, a condition identified as the optimal for Cr(VI) adsorption in the single-component system. Fig. 6b shows that Cd(II) broke through the column within two hours, followed in the order by Cu(II) and Cr(VI). Notably, the Cr(VI) adsorption breakthrough profile exhibited a highly symmetric pattern that still fitted well with the Thomas model ($r^2$ = 0.98), A-B model ($r^2$ = 0.94 for $C_t/C_0$ = 50%) and Y-N model ($r^2$ = 0.98). In contrast, the breakthrough curves of Cu(II) and Cd(II) showed a distinctly different pattern from that of Cr(VI). Not only did Cd(II) completely break through within a period of time, its $C_t/C_0$ value overshot to a value of ~1.25 before stabilizing toward the equilibrium. In contrast, Cu(II) also broke through immediately after the commencement of the column run, then stabilized at $C/C_0$ ~ 0.8 but never reached complete breakthrough. The time it took to reach a $C_t/C_0$ plateau was significantly longer for Cr(VI) than they were for Cu(II) and Cd(II). The longer time to experience a breakthrough suggests that the column favored the Cr(VI) adsorption over the two other metal ions.

The preference of Cr(VI) in the ternary system at pH 4 clearly exhibited a competitive adsorption phenomenon. We hypothesized that the electrosorption between $HCrO_4^-$ and protonated

binding groups ($–COOH_2^+$, $–OH_2^+$, $–NH_3^+$) on CS/MWCNTs/Fe beads dominated the adsorption over chelation ($NH_2 + Cu^{2+}/Cd^{2+} \rightarrow NH_2Cu^{2+}/Cd^{2+}$) or ion exchange ($Ca^{2+}$ with $Cu^{2+}$ and $Cd^{2+}$) that were likely the main adsorption mechanisms for divalent cations. Between Cu(II) and Cd(II), the higher electronegativity (1.95) and smaller hydrated ionic radii (0.419 nm) of Cu(II) might be responsible of its higher adsorption affinity than that of Cd(II) (electronegativity,1.69; hydrated ionic radii, 0.426 nm), leading to a competitive advantage. Furthermore, phosphate as a background anion matrix did not significantly interfere with the adsorption and breakthrough behaviors of Cr(VI) and Cd(II). However, the formation of stable precipitates such as $Cu_3(PO_4)_2$ during the adsorption process is a plausible explanation to why Cu(II) never approached complete breakthrough by monitoring the effluent concentration. Altogether, we present Fig. 6b to illustrate the following process: (i) all three metal ions were adsorbed on CS/MWCNTs/Fe beads at the beginning when unoccupied active sites were abundant; (ii) Adsorption sites occupied by Cd(II) ions were replaced by both Cr(VI) and Cu(II) ions as they continued to be adsorbed; (iii) Cr(VI) ions continued to be adsorbed while Cu(II) attained an equilibrium, (iv) Cr(VI) ions adsorption attained an equilibrium.

## 4 Conclusions

The present study characterizes the performance of CS/MWCNTs/Fe beads for aqueous phase Cr(VI) removal in fixed-bed columns. A maximum volume of treated effluent of 210 mL and an Cr(VI) uptake capacity of 1.52 mg $g^{-1}$ were achieved at 1 mL $min^{-1}$ in flow rate, 8 cm in bed height, 30 mg $L^{-1}$ in feed Cr(VI) concentration and a pH value of 4. Both the Thomas model and Y-N model are well-suited to describe the dynamics of the adsorption breakthrough process of Cr(VI), while the A-B model was applicable only to describe the early phase of the dynamic behavior ($C_t/C_0 \leq 0.5$) of the column. The parameters in the Thomas model and A-B model possess physical

implications that reflect the effects of the various operating parameters (flow rate, initial concentration, and bed height) on the mass transfer rate and adsorption capacity. By successfully characterizing the breakthrough behaviors with the models, we further applied the BDST model for the prediction of system behavior under several hypothetical operating conditions and the subsequent scale-up. We demonstrated that the packed bed dimensions and flow rates determined the amount of adsorbent beads needed to achieve a prescribed breakthrough criterion. We also demonstrated that, when the synthetic solution contained multiple heavy metals, i.e., Cr(VI), Cu(II), and Cd(II), Cr(VI) was selectively adsorbed in the CS/MWCNTs/Fe beads column, and was less impacted by the presence of a background anion in phosphate.

## References


[1] J.C. Almeida, C.E. Cardoso, D.S. Tavares, R. Freitas, T. Trindade, C. Vale, et al., Chromium removal from contaminated waters using nanomaterials – A review, TrAC Trends in Analytical Chemistry. 118 (2019) 277–291. doi:10.1016/j.trac.2019.05.005.

[2] C. Raji, T. Anirudhan, Batch Cr(VI) removal by polyacrylamide-grafted sawdust: Kinetics and thermodynamics, Water Research. 32 (1998) 3772–3780. doi:10.1016/s0043-1354(98)00150-x.

[3] V.E. Pakade, N.T. Tavengwa, L.M. Madikizela, Recent advances in hexavalent chromium removal from aqueous solutions by adsorptive methods, RSC Advances. 9 (2019) 26142–26164. doi:10.1039/c9ra05188k.

[4] F. Fu, Q. Wang, Removal of heavy metal ions from wastewaters: A review, Journal of Environmental Management. 92 (2011) 407–418. doi:10.1016/j.jenvman.2010.11.011.

[5] E. Rodrigues, O. Almeida, H. Brasil, D. Moraes, M.D. Reis, Adsorption of chromium (VI) on hydrotalcite-hydroxyapatite material doped with carbon nanotubes: Equilibrium, kinetic and thermodynamic study, Applied Clay Science. 172 (2019) 57–64. doi:10.1016/j.clay.2019.02.018.

[6] G. Qin, M.J. Mcguire, N.K. Blute, C. Seidel, L. Fong, Hexavalent chromium removal by reduction with ferrous sulfate, coagulation, and filtration: A pilot-scale study, Environmental Science & Technology. 39 (2005) 6321–6327. doi:10.1021/es050486p.

[7] D. Pradhan, L.B. Sukla, M. Sawyer, P.K. Rahman, Recent bioreduction of hexavalent chromium in wastewater treatment: A review, Journal of Industrial and Engineering Chemistry. 55 (2017) 1–20. doi:10.1016/j.jiec.2017.06.040.

[8] L. Lin, X. Xu, C. Papelis, T.Y. Cath, P. Xu, Sorption of metals and metalloids from reverse osmosis concentrate on drinking water treatment solids, Separation and Purification Technology. 134 (2014) 37–45. doi:10.1016/j.seppur.2014.07.008.

[9] M.G. Reddi, T. Gomathi, M. Saranya, P. Sudha, Adsorption and kinetic studies on the removal of chromium and copper onto Chitosan-g-maliec anhydride-g-ethylene dimethacrylate, International

Journal of Biological Macromolecules. 104 (2017) 1578–1585. doi:10.1016/j.ijbiomac.2017.01.142.

[10] V.N. Thekkudan, V.K. Vaidyanathan, S.K. Ponnusamy, C. Charles, S. Sundar, D. Vishnu, et al., Review on nanoadsorbents: a solution for heavy metal removal from wastewater, IET Nanobiotechnology. 11 (2016) 213–224. doi:10.1049/iet-nbt.2015.0114.

[11] G. Ren, X. Wang, P. Huang, B. Zhong, Z. Zhang, L. Yang, et al., Chromium (VI) adsorption from wastewater using porous magnetite nanoparticles prepared from titanium residue by a novel solid-phase reduction method, Science of The Total Environment. 607-608 (2017) 900–910. doi:10.1016/j.scitotenv.2017.06.103.

[12] L. Li, Y. Li, L. Cao, C. Yang, Enhanced chromium (VI) adsorption using nanosized chitosan fibers tailored by electrospinning, Carbohydrate Polymers. 125 (2015) 206–213. doi:10.1016/j.carbpol.2015.02.037.

[13] Y. Li, Y. Gao, Q. Zhang, R. Wang, C. Li, J. Mao, et al., Flexible and free-standing pristine polypyrrole membranes with a nanotube structure for repeatable Cr(VI) ion removal, Separation and Purification Technology. 258 (2021) 117981. doi:10.1016/j.seppur.2020.117981.

[14] A. Mohamed, W.S. Nasser, T.A. Osman, M.S. Toprak, M. Muhammed, A. Uheida, Removal of chromium (VI) from aqueous solutions using surface modified composite nanofibers, Journal of Colloid and Interface Science. 505 (2017) 682–691. doi:10.1016/j.jcis.2017.06.066.

[15] J.H. Chang, J. Kim, H. Lee, PNIPAm grafted amino-functionalized mesoporous silica for thermo-responsive chromium elimination, Applied Surface Science. 424 (2017) 115–121. doi:10.1016/j.apsusc.2017.01.168.

[16] L. Li, H. Duan, X. Wang, C. Luo, Adsorption property of Cr(vi) on magnetic mesoporous titanium dioxide–graphene oxide core–shell microspheres, New J. Chem. 38 (2014) 6008–6016. doi:10.1039/c4nj00782d.

[17] M.M.A. Aslam, W. Den, H.-W. Kuo, Encapsulated chitosan-modified magnetic carbon nanotubes for aqueous-phase CrVI uptake, Journal of Water Process Engineering. (2020) 101793. doi:10.1016/j.jwpe.2020.101793.

[18] K. Vijayaraghavan, J. Jegan, K. Palanivelu, M. Velan, Batch and column removal of copper from aqueous solution using a brown marine alga Turbinaria ornata, Chemical Engineering Journal. 106 (2005) 177–184. doi:10.1016/j.cej.2004.12.039.

[19] M. Bhaumik, K. Setshedi, A. Maity, M.S. Onyango, Chromium(VI) removal from water using fixed bed column of polypyrrole/Fe3O4 nanocomposite, Separation and Purification Technology. 110 (2013) 11–19. doi:10.1016/j.seppur.2013.02.037.

[20] H.C. Thomas, Heterogeneous ion exchange in a flowing system, Journal of the American Chemical Society. 66 (1944) 1664–1666. doi:10.1021/ja01238a017.

[21] R. Han, Y. Wang, W. Zou, Y. Wang, J. Shi, Comparison of linear and nonlinear analysis in estimating the Thomas model parameters for methylene blue adsorption onto natural zeolite in fixed-bed column, Journal of Hazardous Materials. 145 (2007) 331–335. doi:10.1016/j.jhazmat.2006.12.027.

[22] G.S. Bohart, E.Q. Adams, Some aspects of the behavior of charcoal with respect to chlorine.1, Journal of the American Chemical Society. 42 (1920) 523–544. doi:10.1021/ja01448a018.

[23] S. Chen, Q. Yue, B. Gao, Q. Li, X. Xu, K. Fu, Adsorption of hexavalent chromium from aqueous solution by modified corn stalk: A fixed-bed column study, Bioresource Technology. 113 (2012) 114–120. doi:10.1016/j.biortech.2011.11.110.

[24] Y.H. Yoon, J.H. Nelson, Application of gas adsorption kinetics I. A theoretical model for respirator cartridge service life, American Industrial Hygiene Association Journal. 45 (1984) 509–516. doi:10.1080/15298668491400197.

[25] A. Singh, D. Kumar, J. Gaur, Continuous metal removal from solution and industrial effluents using Spirogyra biomass-packed column reactor, Water Research. 46 (2012) 779–788. doi:10.1016/j.watres.2011.11.050.

[26] Z. Marczenko, M. Masson, Separation and spectrophotometric determination of elements, Horwood, Chichester, 1986.

[27] M.A. Fulazzaky, Determining the resistance of mass transfer for adsorption of the surfactants onto granular activated carbons from hydrodynamic column, Chemical Engineering Journal. 166 (2011) 832–840. doi:10.1016/j.cej.2010.11.052.

[28] M.A. Fulazzaky, M.H. Khamidun, M.F.M. Din, A.R.M. Yusoff, Adsorption of phosphate from domestic wastewater treatment plant effluent onto the laterites in a hydrodynamic column, Chemical Engineering Journal. 258 (2014) 10–17. doi:10.1016/j.cej.2014.07.092.

[29] G. Rexwinkel, A.B.M. Heesink, W.P.M. Van Swaaij, Mass transfer in packed beds at Low Peclet numbers—wrong experiments or Wrong interpretations?, Chemical Engineering Science. 52 (1997) 3995–4003. doi:10.1016/s0009-2509(97)00242-x.

[30] C.A. Demarchi, A. Debrassi, J.D. Magro, N. Nedelko, A. Ślawska-Waniewska, P. Dłużewski, et al., Adsorption of Cr(VI) on crosslinked chitosan–Fe(III) complex in fixed-bed systems, Journal of Water Process Engineering. 7 (2015) 141–152. doi:10.1016/j.jwpe.2015.05.003.

[31] W. Wang, M. Li, Q. Zeng, Adsorption of chromium (VI) by strong alkaline anion exchange fiber in a fixed-bed column: Experiments and models fitting and evaluating, Separation and Purification Technology. 149 (2015) 16–23. doi:10.1016/j.seppur.2015.05.022.

[32] M. Basu, A.K. Guha, L. Ray, Adsorption of lead on Lentil husk in fixed bed column bioreactor, Bioresource Technology. 283 (2019) 86–95. doi:10.1016/j.biortech.2019.02.133.

[33] A. Ramírez, S. Giraldo, J. García-Nunez, E. Flórez, N. Acelas, Phosphate removal from water using a hybrid material in a fixed-bed column, Journal of Water Process Engineering. 26 (2018) 131–137. doi:10.1016/j.jwpe.2018.10.008.

[34] S. Chatterjee, S. Mondal, S. De, Design and scaling up of fixed bed adsorption columns for lead removal by treated laterite, J. Cleaner Production. 177 (2018) 760–774. doi:10.1016/j.jclepro.2017.12.249.

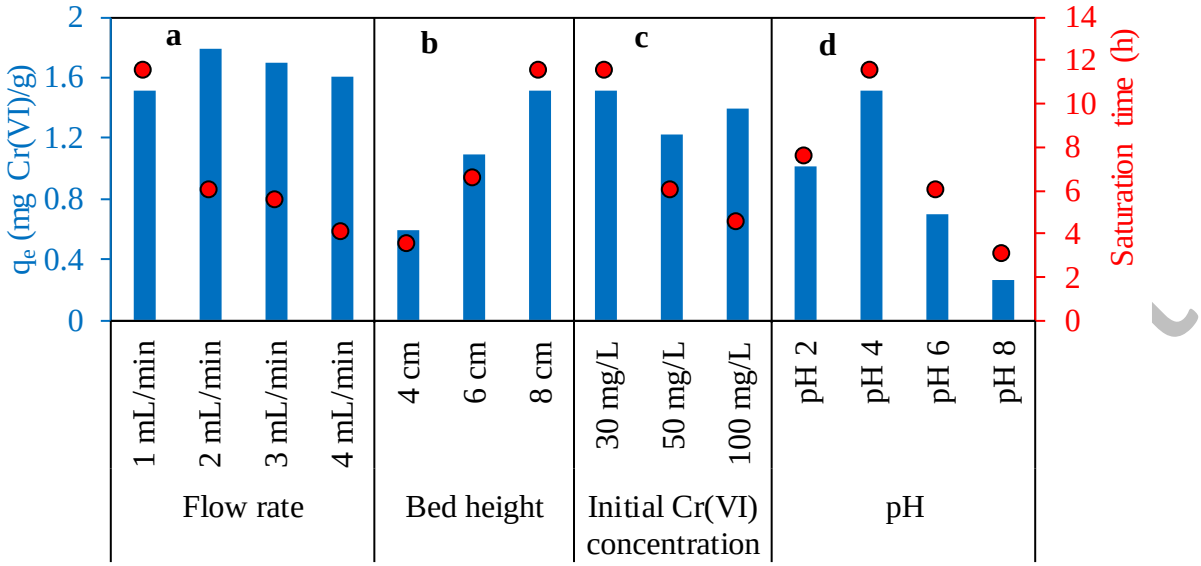


Fig. 1. Measured adsorption capacity and saturation time (a) different column flow rates (feed Cr(VI) concentration, 30 mg $L^{-1}$; bed depth, 8 cm; solution pH, 4±0.2), (b) different bed heights (feed Cr(VI) concentration, 30 mg $L^{-1}$; flow rate, 1 mL $min^{-1}$; solution pH, 4±0.2), (c) different inlet Cr(VI) concentrations (flow rate, 1 mL $min^{-1}$; bed depth, 8 cm; solution pH, 4±0.2), and (d) different solution pH values (feed Cr(VI) concentration, 30 mg $L^{-1}$; flow rate, 1 mL $min^{-1}$; bed depth, 8 cm).

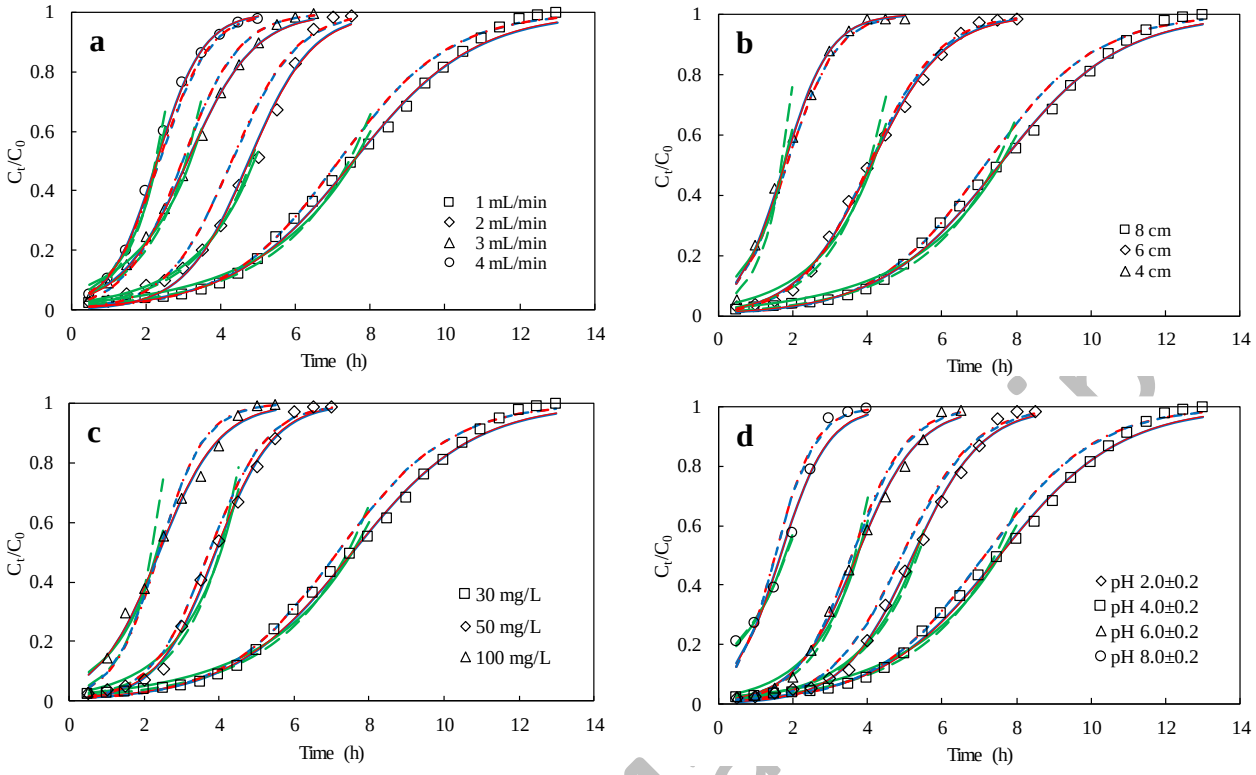


Fig. 2. Breakthrough profile of Cr(VI) adsorption with Thomas model (blue curve), Yoon-Nelson model (red curve) and Adams-Bohart model (green curve) at (a) different column flow rates (feed Cr(VI) concentration, 30 mg $L^{-1}$; bed depth, 8 cm; solution pH, 4±0.2), (b) different bed depths (feed Cr(VI) concentration, 30 mg $L^{-1}$; flow rate, 1 mL $min^{-1}$; solution pH, 4±0.2), (c) different inlet Cr(VI) concentrations (flow rate, 1 mL $min^{-1}$; bed depth, 8 cm; solution pH, 4±0.2), and (d) different solution pH values (flow rate, 1 mL $min^{-1}$; feed Cr(VI) concentration, 30 mg $L^{-1}$; bed depth, 8 cm). All solid lines refer to non-linear fittings and dashed line to linearized fittings.

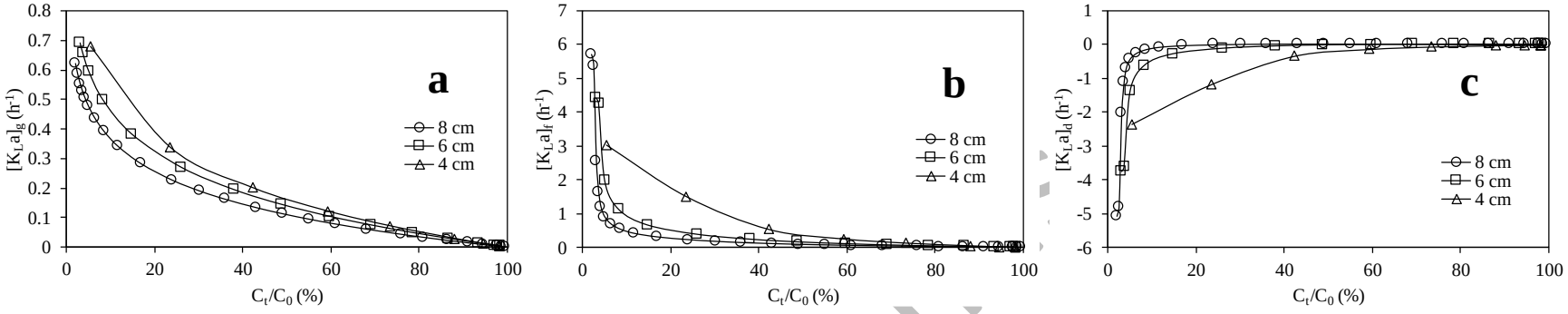


Fig. 3. Variations of the controlling mass transport factors in accordance with the percentage of outflow (a) global, (b) film and (c) pore diffusion for Cr(VI) adsorption onto CS/MWCNTs/Fe beads at varying bed depths (flow rate, 1 $mLmin^{-1}$; feed Cr(VI) concentration, 30 $mg\ L^{-1}$; solution pH, 4±0.2)

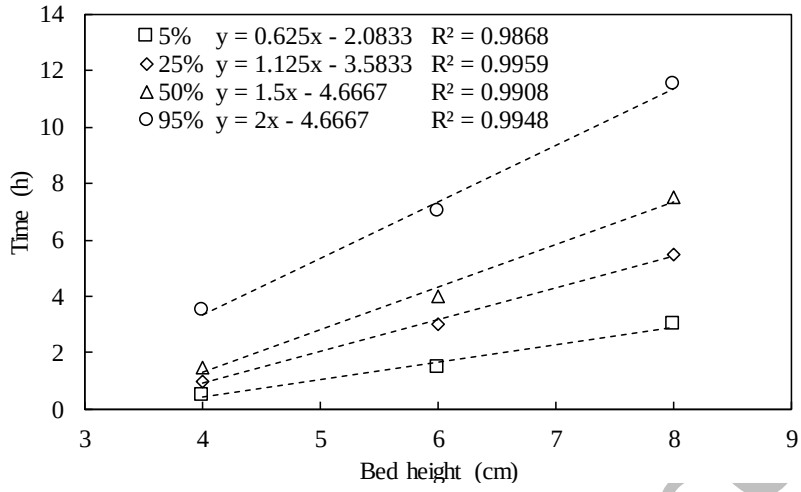


Fig. 4. BDST best-fit lines at $C_t/C_0$ =5, 25, 50, and 95% with different bed depths (flow rate; 1 mL $min^{-1}$, feed Cr(VI) concentration; 30 mg $L^{-1}$, and pH; 4±0.2).

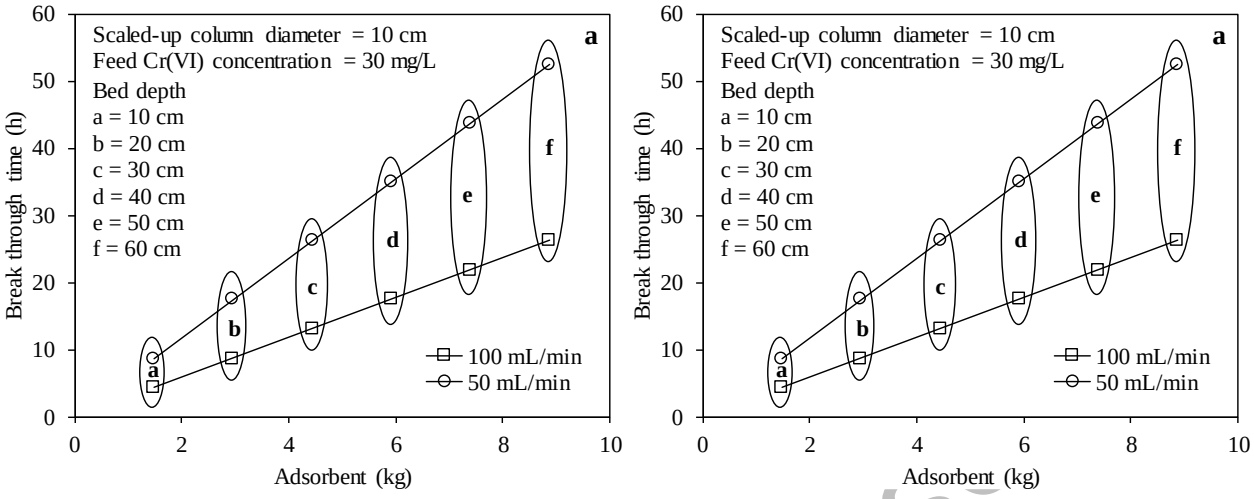


Fig. 5. Estimation of the amount of CS/MWCNTs/Fe beads required to pack into upscaled continuous column and corresponding breakthrough time at (a) different bed depth and constant column diameter and (b) different column diameter and constant bed depth.

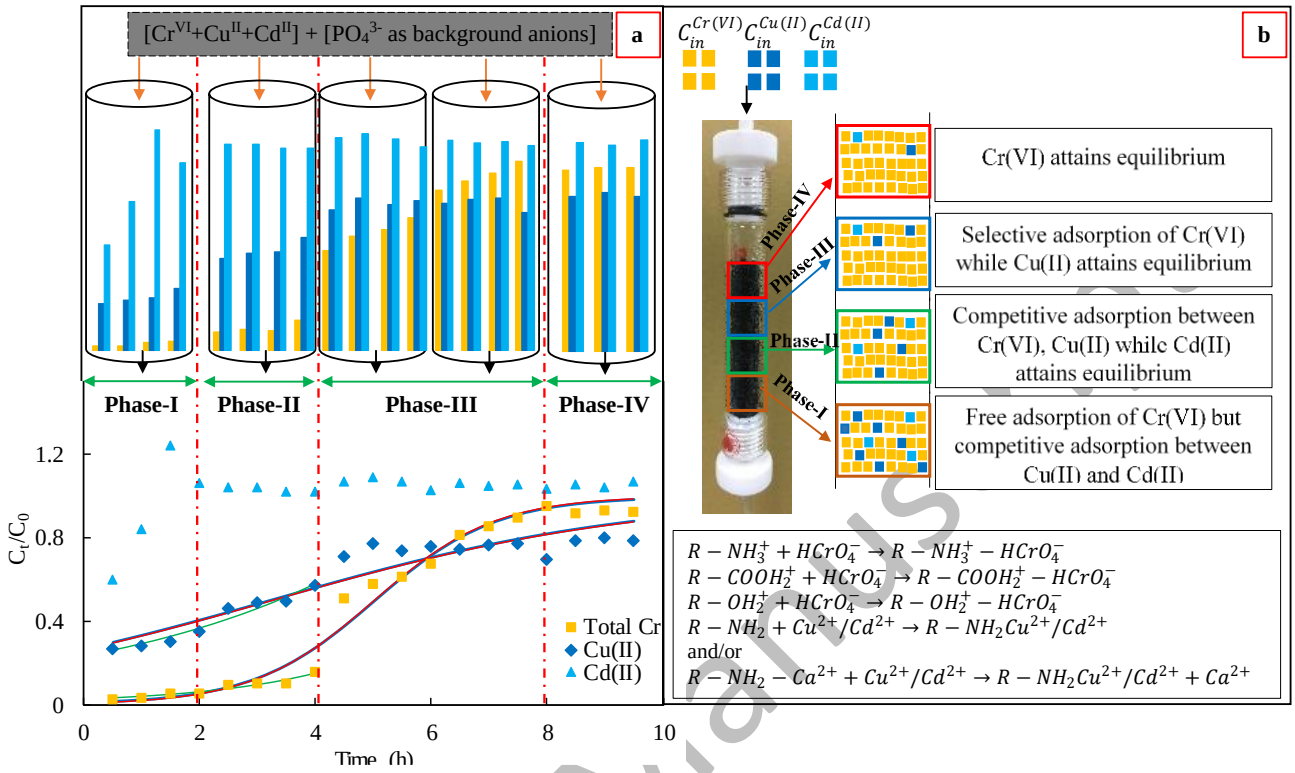


Fig. 6. Application of CS/MWCNTs/Fe beads for Cr(VI), Cu(II) and Cd(II) adsorption in ternary fixed-bed column system (a) fitted breakthrough profile with experimental data (b) pattern of metal ions adsorption (flow rate 1 mL $min^{-1}$; feed concentration of Cr(VI), Cu(II) and Cd(II) 1 mg $L^{-1}$ each; bed depth 8 cm; solution pH 4±0.2; background $PO_4^{3-}$ anions 30 mg $L^{-1}$).

Table 1. The empirical breakthrough models fitted with experimental data.

| Model | Governing equation | Key assumptions & characteristics |
|---|---|---|
| Thomas | $\frac{C_t}{C_0} = \frac{1}{1+\exp\left(\frac{k_{TH}q_0W}{Q} - k_{TH}C_0t\right)}$<br>Linear form:<br>$\mathrm{Ln}\left(\frac{C_t}{C_0} - 1\right) = \frac{k_{TH}q_0W}{Q} - k_{TH}C_0t$ | • Adsorption process is not only controlled by chemical interaction but also by interface mass transfer.<br>• Follows Langmuir isotherms and second-order adsorption kinetics. |
| Adam-Bohart | $\frac{C_t}{C_0} = \exp\left(k_{AB}C_0t - \frac{k_{AB}N_{AB}Z}{v}\right)$<br>Linear form:<br>$\mathrm{Ln}\left(\frac{C_t}{C_0}\right) = k_{AB}C_0t - \frac{k_{AB}N_{AB}Z}{v}$ | • The rate of adsorption process is continuous, influenced by film mass transfer and equilibrium does not occur instantaneously.<br>• Generally fitted to investigate early phase of breakthrough curve $\left(\frac{C_t}{C_0} \leq 0.5\right)$. |
| Yoon-Nelson | $\frac{C_t}{C_0} = \frac{1}{1+e^{k_{YN}(\tau - t)}}$<br>Linear form:<br>$\mathrm{Ln}\left(\frac{C_t}{C_0 - C_t}\right) = k_{YN}t - \tau k_{YN}$ | • The decrease in adsorption probability of adsorbates is proportional to probability of adsorption of adsorbate and breakthrough onto the adsorbent<br>• Measures the errors produced by Thomas model. No physicochemical properties of adsorbent and adsorption bed are required. |
| BDST | $t = \frac{N_0Z}{C_0v} - \frac{1}{k_BC_0}\mathrm{Ln}\left(\frac{C_0}{C_t} - 1\right)$ | • Linear relation between the bed height and the operating time of the packed bed column.<br>• Negligible internal diffusion and film mass transfer resistance.<br>• Gives an adequate estimate to the lowest column depth for a limited degree of saturation. |

Notation:
t: service time of packed bed (h); $C_0$: influent concentration (mg $L^{-1}$); $C_t$: effluent concentration at t (mg $L^{-1}$); $q_0$: maximum adsorbate concentration in solid form (mg $g^{-1}$); W: packed amount of adsorbent (g); Z: bed depth (cm); v: linear velocity (cm $min^{-1}$); $N_{AB}$: maximum adsorption capacity per column volume (mg $L^{-1}$); $k_{TH}$: Thomas rate constant (L $mg^{-1}$ $h^{-1}$); $k_{AB}$: Adams-Bohart mass transfer constant (L $mg^{-1}$ $h^{-1}$); $k_{YN}$: Yoon-Nelson rate constant ($h^{-1}$); $\tau$: the time needed to achieve 50% of breakthrough (h); $k_B$: rate constant of BDST model (L $mg^{-1}$ $h^{-1}$); $N_0$: adsorption capacity per volume (mg $L^{-1}$)